Simultaneous PLIF/PIV Investigation of Vortex-Flame Interactions

T. R. Meyer, G. J. Fiechtner, C. D. Carter, J. R. Gord, S. P. Gogineni

Abstract Recent studies of vortex-flame interactions have advanced the understanding of isolated turbulent events and their impact on local non-premixed flame fronts. In the current investigation, vortex-flame interactions in a counterflow Rolon Burner developed at École Centrale Paris/CNRS are investigated using a simultaneous PLIF/PIV technique. The hydroxyl (OH) layer produced by a hydrogen-air flame is imaged using planar laser-induced fluorescence (PLIF), and vortex-characterization data are acquired using two-color digital particle-image velocimetry (PIV). Experiments are performed for cases with and without flame extinction. Results show that the case with flame extinction has higher initial vortex strength but experiences greater levels of energy dissipation at later times due to flame propagation within the vortex rollers. Measurements at high temporal resolution show that the extinction process takes place in an annular region at the leading edge of the vortex rather than at the centerline for the conditions investigated in the present experiment. Local normal strain rates computed from the PIV data showed higher *fuel-side* normal strain rates in the annular region of the vortex-perturbed flame, but higher *air-side* normal strain rates at the centerline.

1 Introduction

Recent results of numerical-modeling efforts combined with advanced laser-diagnostic measurements have led to important advances in the understanding of combustion. Numerous investigations have contributed to these advances, including a particular type of study in which the interaction of a laminar, nonpremixed flame and a vortex is examined. The resulting data can be used for a variety of purposes, such as identifying fundamental regimes of vortex-flame interactions (Katta et al. 1998, Fiechtner et al. 2000, Renard et al. 2000). It is well recognized that vortices occur readily in turbulent flows. Vortical structures play an important role in unsteady and turbulent combustion, and experimental data can be used to develop models in combustion areas such as experimental gas-turbine combustors. Experimental study of vortical structures is difficult because of the need to isolate those structures in space and time with respect to a flame front. Therefore, experiments in which a feature of turbulence is isolated and studied are valuable in furthering the understanding of combustion processes, leading to numerous experimental studies of vortex-flame interactions.

Particle-Image Velocimetry (PIV) is an established technique which is being applied to a wide variety of flows including combustion. Planar Laser-Induced Fluorescence (PLIF) has also been in use for a number of years. Recently, several researchers conducted joint PLIF/PIV experiments in flames. Mueller et. al. (1995) performed PIV and OH-PLIF experiments on repeatable vortex-flame interactions. Frank et. al. (1996) reported simultaneous scalar- and velocity-field measurements in turbulent gas-phase flows. Hasselbrink et al. (1997) made simultaneous planar velocity and OH-fluorescence measurements at the base of a lifted, non-premixed, transverse methane jet flame. Rehm & Clemens (1997) made OH-PLIF and PIV measurements in a hydrogen jet flame. Donbar et al. (1998) made simultaneous CH-PLIF and PIV measurements in turbulent flames. Watson et al. (1999) performed scalar- and velocity-field measurements in lifted methane-air diffusion flames. In the present paper, simultaneous OH-PLIF and PIV measurements are made in an opposed-jet Rolon Burner developed at École Centrale Paris/CNRS. A precise control of the relative timing between the laser diagnostics and the vortex-flame event was implemented to explore the time-dependent nature of the vortex-flame interactions.

2 Burner Facility

A schematic of the opposed-jet Rolon Burner is shown in Fig. 1. The flame is supported between upper and lower nozzles that are separated by 40 mm; each nozzle has an exit diameter of 25 mm. The fuel consists of hydrogen

T. R. Meyer, G. J. Fiechtner, C. D. Carter, S. P. Gogineni
Innovative Scientific Solutions Inc., Dayton OH, 45440 USA

J. R. Gord
Air Force Research Laboratory, Propulsion Directorate, Wright Patterson AFB, OH, 45433 USA

Correspondence to:
S. P. Gogineni
Innovative Scientific Solutions. Inc.
2766 Indian Ripple Road, Dayton OH, 45440 USA
Sivaram.gogineni@wpafb.af.mil

diluted with nitrogen and flows from the upper nozzle; air flows from the lower nozzle. A flow of air is supplied to a vortex tube such that in the absence of a vortex, the exit velocity matches the velocity of the air emanating from the surrounding nozzle. Many types of vortices can be produced experimentally, including isolated single vortices and groups of multiple coaxial vortices. As fluid is pumped impulsively from a nozzle or orifice, a single vortex forms, followed by additional vortices in the production of a starting jet. The vortex generator used in the present study can sweep a maximum volume of ~3 cm^3, for a maximum attainable L/D ratio of ~30. For the experiments described here, comparatively strong vortices are generated using a 0.1-ms piston rise-time.

Vortex formations are monitored carefully to avoid the multiple-vortex condition by examining scattering images that are acquired with a color digital camera. Since vortices that are laminar initially can become unsteady and turbulent, these conditions are also avoided in the present study. In addition, the piston/cylinder is aligned and lubricated properly to avoid situations in which an undesired turbulent column of fluid exits the tube. Vortex visualization is accomplished during alignment of the vortex nozzle using PLIF of acetone.

Seed particles are introduced into the burner flows when digital PIV measurements of the vortex velocity are performed. Three particle seeders are installed—one after the air mass-flow controller, a second after the vortex-air mass-flow controller, and a third after the junction where the hydrogen and nitrogen gases are mixed. With the use of three seeders, each flow can be seeded with particles individually, or combinations of the different flowfields can be seeded. Each seeder contains hollow spherical ceramic particles with an approximate mean diameter of 2.4 μm. When PIV studies are not required, the seeders are removed from the apparatus. Experiments are repeated for both seeded and unseeded flows, and no significant change in the results is caused by the presence of seed particles.

Synchronization and Timing

Since data on the time-dependent nature of the vortex-flame interactions are to be compared with computational predictions (in addition to spatial-feature comparisons), precise synchronization of several experimental events is required, including generation and propagation of vortices, production of laser pulses, and activation of the camera shutter and intensifier. A block diagram of the synchronization scheme is shown in Fig. 2. The scheme depicted here provides precise control of the relative timing between the laser diagnostics and the vortex-flame event. To explore the temporal evolution of the event, data are captured utilizing the following phase-locked timing sequence: 1) an image is recorded, 2) the delay between vortex production and the laser/camera events is adjusted, and 3) another vortex is initiated and a second image recorded. This process is repeated to acquire numerous images that are obtained at increasing delays.

3
Measurement Techniques and Data Collection

The PLIF system contains a frequency-doubled, Q-switched Nd:YAG laser that is used to pump a dye laser; this dye laser, in turn, is frequency doubled. The UV radiation is directed through a telescope that is adjusted to produce a light sheet with a height that matches as nearly as possible the 40-mm burner separation. The resulting beam thickness is ~300 μm, which corresponds to the full width (defined as the distance between the locations of the 25%-peak-intensity points).

Hydroxyl radicals absorb the laser radiation at 281.3414 nm via the $R_1(8)$ transition of the (1,0) band in the A-X system. Fluorescence from the A-X (1,1) and (0,0) bands is detected at right angles through WG-295 and UG-11 colored-glass filters using a 105-mm-focal-length f/4.5 UV lens. The resulting light is recorded on an intensified CCD camera with an intensifier gate width of 100 ns. CCD pixels are binned in 2 x 2 groups; the result is an effective array size of 288 x 192 pixels, with an imaged area of 25.6 x 38.4 mm^2. The bottom of the image is flush with the surface of the lower nozzle. A color table is used, with a maximum value set to 95% of the maximum signal for all images taken at a given flame condition. The low-signal color is assigned by calculating the mean background noise and selecting a minimum value that is at least two standard deviations above this level.

Measurements of the velocity field are carried out using two-color digital PIV (Gogineni et al. 1998). A color digital CCD with an array of 3060 x 2036 pixels is used. A magnification of 78 pixels/mm results in an imaged area of 26.0 x 39.0 mm^2. The color CCD camera and the intensified CCD array are aligned using a transparent mask printed with a graduated scale. Further alignment between images is performed after each experiment employing software; a transformation in two-dimensional space is applied to the PIV images relative to the PLIF images. Two lasers are used, with one PIV light sheet produced by frequency doubling the output of a Q-switched Nd:YAG laser (30 mJ/pulse at the test section). The remainder of this beam is used to pump the dye laser that is frequency doubled

to excite OH fluorescence. The second PIV light sheet is produced by pumping a dye laser (employing DCM laser dye) with a second frequency-doubled, Q-switched Nd:YAG laser; this results in laser radiation at 640 nm (40 mJ/pulse at the test section). The thickness of both the red and the green light sheets is set to ~700 μm at the probe region. A digital delay generator is used to drive the timing of the two lasers such that the red pulses are delayed precisely with respect to the green ones. In the absence of a vortex, the underlying counterflow velocity field is probed with red pulses that are delayed by up to 1 ms with respect to the corresponding green pulses. For the fastest vortices studied, the delay between red and green pulses is reduced to 10 μs. The camera shutter is set to open for 1/15 s to permit detection of both laser pulses by the color CCD. Flame emission and light from other devices in the laboratory (monitors, etc.) are attenuated greatly by the shutter.

Velocity vectors are calculated using the custom designed software developed at Stanford (Stan PIV – Hasselbrink 1999). This software incorporates several improvements to standard (single-pass) PIV algorithms and allows recursive estimation of the velocity field. Spurious vectors are filtered using a consistency filter that rejects vectors that are not within a prescribed radius of a prescribed number of the nearest 8 neighboring vectors. The values of the vectors which are invalidated by the filter are interpolated.

4 Results

Figures 3 and 4 show simultaneous images of OH PLIF overlaid with instantaneous velocity vectors from PIV for cases with no flame extinction and with flame extinction, respectively. All OH PLIF images are normalized to the same color scale and represent qualitative OH concentrations. The velocity vectors plotted here correspond to the reference frame of the vortex and are obtained by subtracting its convection velocity. Figures 3 and 4 also show vorticity distributions computed by central differencing of the velocity field.

For the case with no flame extinction, shown in Fig. 3, the vortex velocity is estimated to be 2 m/s, and the spacing is 9 ms between images. As the vortex impinges upon the flame [Fig. 3(a)], the flame surface is wrinkled and wraps around the leading edge of the vortex. The flame then burns through the vortex rollers without being extinguished [see central and rightmost frames of Fig. 3(a)]. The location of the vortex structure is shown more clearly in the vorticity plots of Fig. 3(b). For the case with flame extinction [Fig. 4], the vortex velocity is estimated to be 3 m/s. In order to ensure that each vortex image in Fig. 4 is at the same stage of development as that of Fig. 3, the time spacing is set to 6 ms between frames. However, the vortex shown in Fig. 4(a) breaks the OH layer as it advances toward the upper nozzle. After this initial extinction, the flame propagates into the vortex rollers and begins to reconnect.

The following is a frame-by-frame comparison of Fig. 3 and 4. The plot of vorticity in the *leftmost* frame of Fig. 4(b) shows that the vortex is stronger relative to that of Fig. 3(b). The vortex in the *central frame* of Fig. 4(b) maintains its strength due to early flame extinction, while the vortex in the corresponding frame in Fig. 3(b) is dissipated due to interaction with the flame. In the *rightmost frame* of Fig. 4(b), the vortex is clearly dissipated as the flame propagates into the roller structures. Interestingly, by comparison, the vortex rollers in the rightmost frames of Fig. 3 are less dissipated than those of Fig. 4. This indicates that flame propagation along the vortex rollers plays a more significant role in the dissipation of vorticity when compared with lateral flame propagation across the vortex in Fig. 3.

To explore the flame extinction process further, simultaneous OH PLIF and velocity vectors are plotted with higher temporal resolution (0.3 ms between frames) in Fig. 5. This clearly shows that flame extinction begins in an annular region near the leading edge of the vortex rather than at the centerline. This phenomenon was first observed in the computational results of Katta et al. (1998).

To evaluate further the effect of strain rate on flame extinction, Fig. 6(a) compares the relative OH PLIF signal with the velocity gradient normal to the flame surface (dU/dR) using data from the leftmost image of Fig. 5, where U and R are the velocity and spatial components, respectively, normal to the flame surface. Both the OH PLIF signal and dU/dR are plotted at various points along the center of the OH layer from Point A to C; the velocity gradient is calculated using a combination of central differencing and linear interpolation between grid points. According to the plot of relative OH signal in Fig. 6(a), flame extinction begins to occur near Point B within a region of maximum dU/dR and away from the jet centerline. Because the center of the OH layer does not mark the stoichiometric surface, line plots of dU/dR across Points A and B are shown for comparison in Fig. 6(b). The peak normal strain rate toward the fuel side is higher in the annular region than at the centerline, while the peak normal strain rate toward the air side is higher at the centerline than in the annular region. This supports the findings of Katta et al. (1998), who suggested that the vortex-induced strain rate is not totally responsible for quenching in the latter

location. Also in agreement with Katta et al. (1998), the fuel side peak normal strain rates shown in Fig. 6(b) are within 10% of the calculated values. The computed air side peak normal strain rates show the correct trends, but are higher than the experimental values by 50-100%. These errors may result from slight errors in PIV-OH image matching, relative resolution, thermophoresis, and particle slip. A detailed analysis of these sources of error is the subject of ongoing investigation.

5 Conclusions

A simultaneous OH PLIF and PIV experiment was performed to explore vortex-flame interactions using a counterflow Rolon Burner with a hydrogen-air diffusion flame. PIV images were collected using a high-resolution, two-color CCD sensor and were processed using a recursive estimation technique for higher vector density. It was demonstrated that PIV is extremely valuable when studying vortex dynamics in the presence of a flame front (as marked by OH PLIF) for cases with and without flame extinction. Plots of vorticity show that the case with flame extinction had higher initial vortex strength but experiences greater levels of dissipation at later times due to flame propagation within the vortex rollers. PIV results were also used to compute local normal strain rates and show very good agreement with computational results from the literature.

Acknowledgments

The authors would like to thank Dr. W. M. Roquemore and Dr. V. R. Katta for their guidance and valuable discussions. The authors also thank Dr. R. D. Hancock and Capt. I. Vihinen for assistance in assembly of the burner and Mr. K. D. Grinstead and Dr. J. M. Donbar for technical assistance in setting up the experiments. Finally, the authors thank Prof. Mungal of Stanford University for providing the StanPIV software. This work is supported by U. S. Air Force Contracts F33615-95-C-2507, F33615-97-C-2702, and F33615-00-C-2608.

References

Donbar, J.M.; Driscoll, J.F.; Carter, C.D. (1998) Simultaneous CH Planar Laser-Induced Fluorescence and Particle Image Velocimetry in Turbulent Flames. AIAA 36th Aerospace Sciences Meeting & Exhibit, Jan. 12-15, 1998, Reno, NV, U.S.A. (AIAA 98-0151).

Fiechtner, G.J.; Renard, P.H.; Carter, C.D.; Gord, J.R.; Rolon, J.C. (2000). Journal of Visualization, Vol. 2, No. 3/4, pp. 331-342.

Frank, J.H.; Lyons, K.M.; Long, M.B. (1996) Simultaneous Scalar/Velocity Field Measurements in Turbulent Gas-Phase Flows. Combustion and Flame, Vol. 107, pp. 1-12.

Gogineni, S.; Goss, L.; Pestian, D.; Rivir, R. (1998) Two-Color Digital PIV Employing a Single CCD Camera. Experiments in Fluids, Vol. 25, pp. 320-328.

Hasselbrink, E. (1999) Transverse Jets and Jet Flames: Structure, Scaling, and Effects of Heat Release. Technical Report TSD-121, Dept. of Mechanical Engg., Stanford University, Stanford, CA

Hasselbrink, E.; Mungal, M.; Hanson, R. (1997) Planar Velocity Measurements and OH Imaging in a Transverse Jet. AIAA 35th Aerospace Sciences Meeting & Exhibit, Jan. 6-10, 1997, Reno, NV, U.S.A. (AIAA 97-0118).

Katta, V.R.; Carter, C.D.; Fiechtner, G.J.; Roquemore, W.M.; Gord, J.R.; Rolon, J.C. (1998). 27th Symposium (International) on Combustion, The Combustion Institute, pp.587-594.

Mueller, C.J. et. al. (1995) Effect of Unsteady Stretch Rate on OH Chemistry during a Flame-Vortex Interaction: to assess Flame Models. Combustion and Flame, Vol. 100, pp. 323-331.

Rehm, J.E.; Clemens, N.T. (1997) A PIV/PLIF Investigation of Turbulent Planar Non-Premixed Flames. AIAA 35th Aerospace Sciences Meeting & Exhibit, Jan. 6-10, 1997, Reno, NV, U.S.A. (AIAA 97-0250).

Renard, P.H.; Thevenin, D.; Rolon, J.C.; Candel, S. (2000) Progress Energy Combustion and Science, Vol. 26, pp. 225-282.

Watson, K.A.; Lyons, K.M.; Donbar, J.M.; Carter, C.D. (1999) Scalar and Velocity Field Measurements in a Lifted CH_4-Air Diffusion Flame. Combustion and Flame, Vol. 117, pp. 257-271.

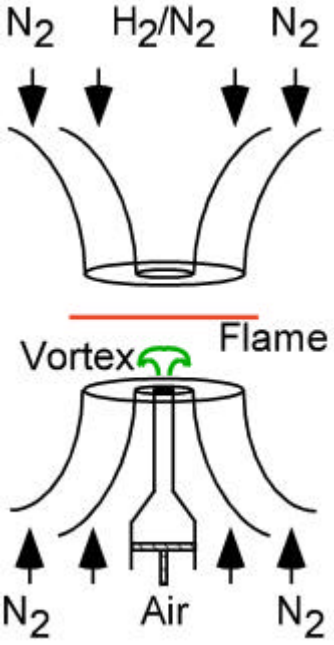

Fig. 1 Schematic of the Rolon Burner.

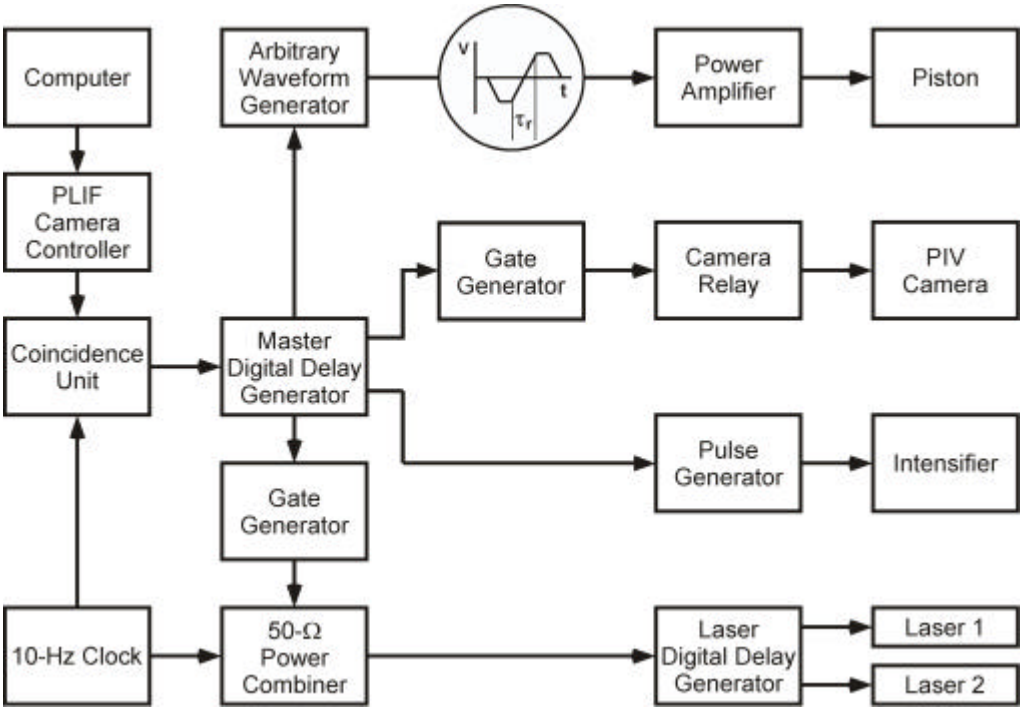

Fig. 2 Block diagram of the synchronization scheme.

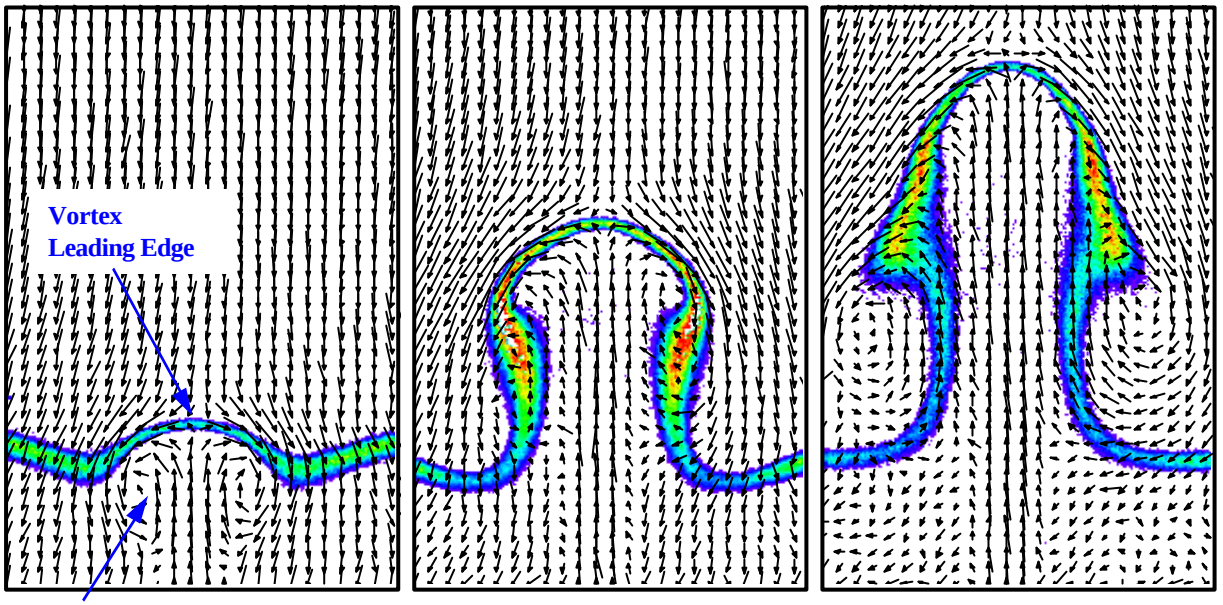

(a)

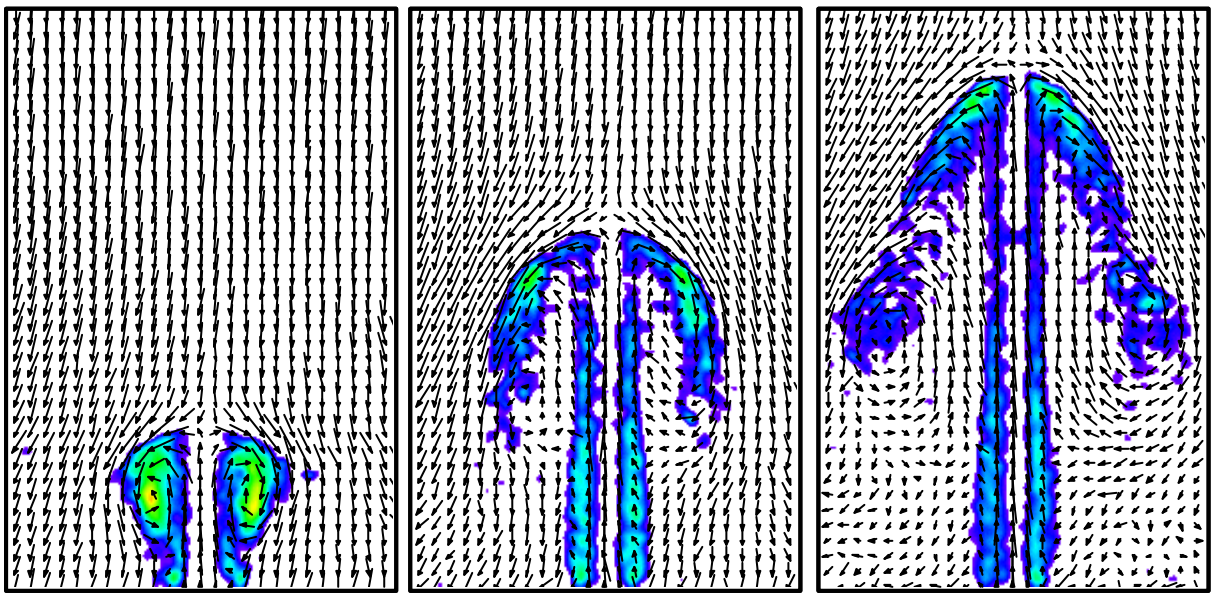

(b)

Fig. 3 (a) Simultaneous OH-PLIF and velocity distributions and (b) superposed velocity and vorticity distributions for a case with no flame extinction. Images progress in time from left to right and are spaced 9 ms apart.

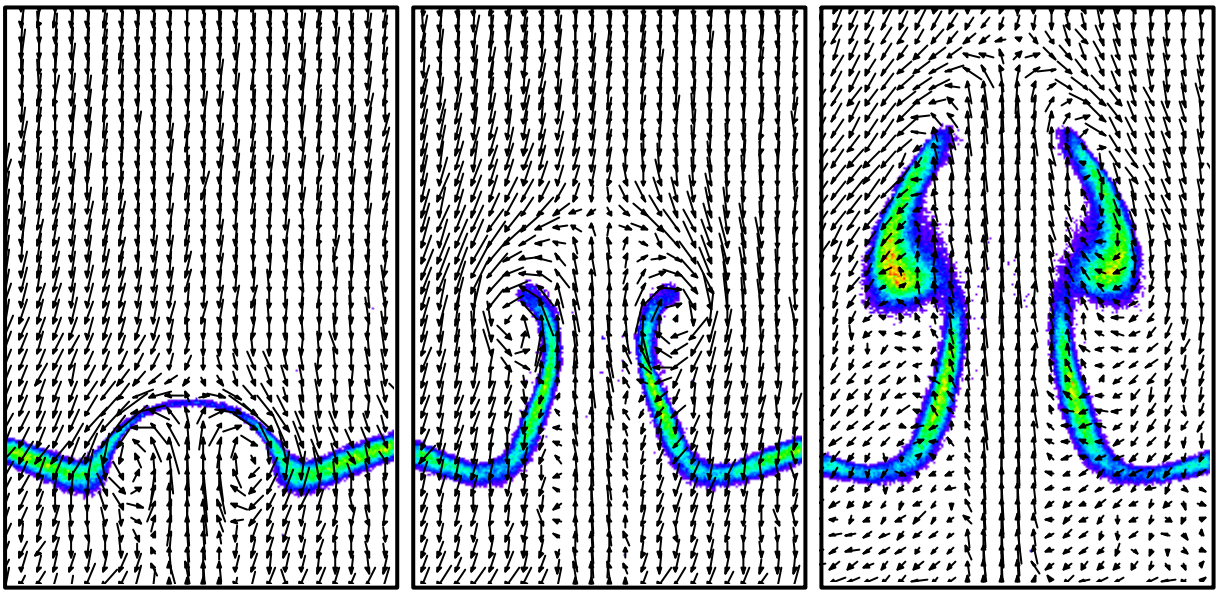

(a)

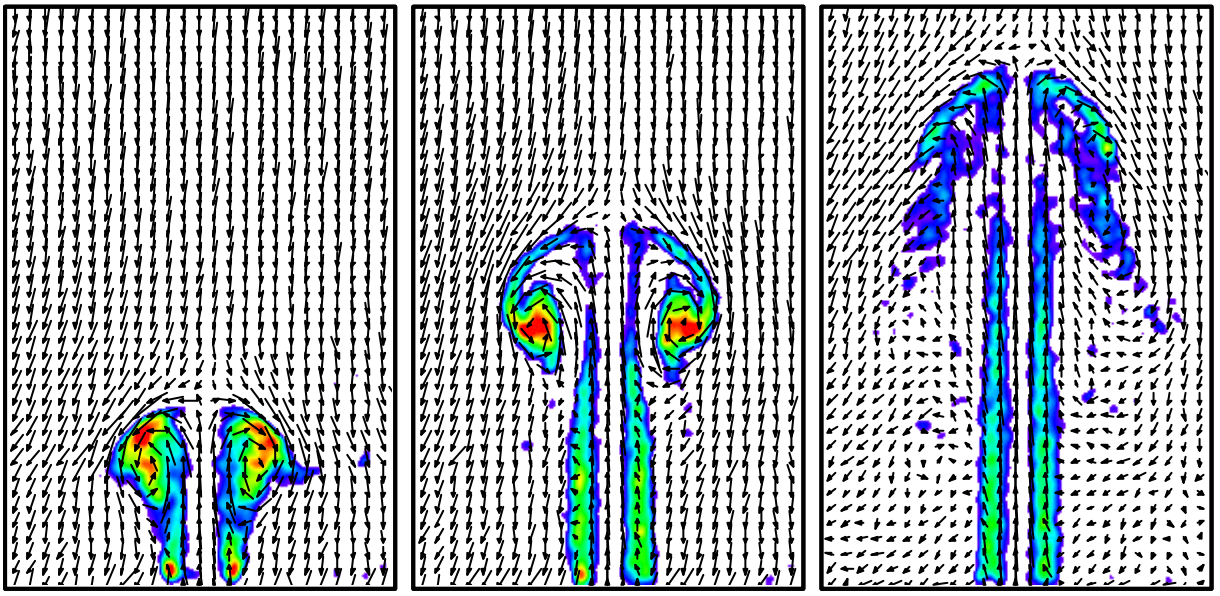

(b)

Fig. 4 (a) Simultaneous OH-PLIF and velocity distributions and (b) superposed velocity and vorticity distributions for a case with flame extinction. Images progress in time from left to right and are spaced 6 ms apart.

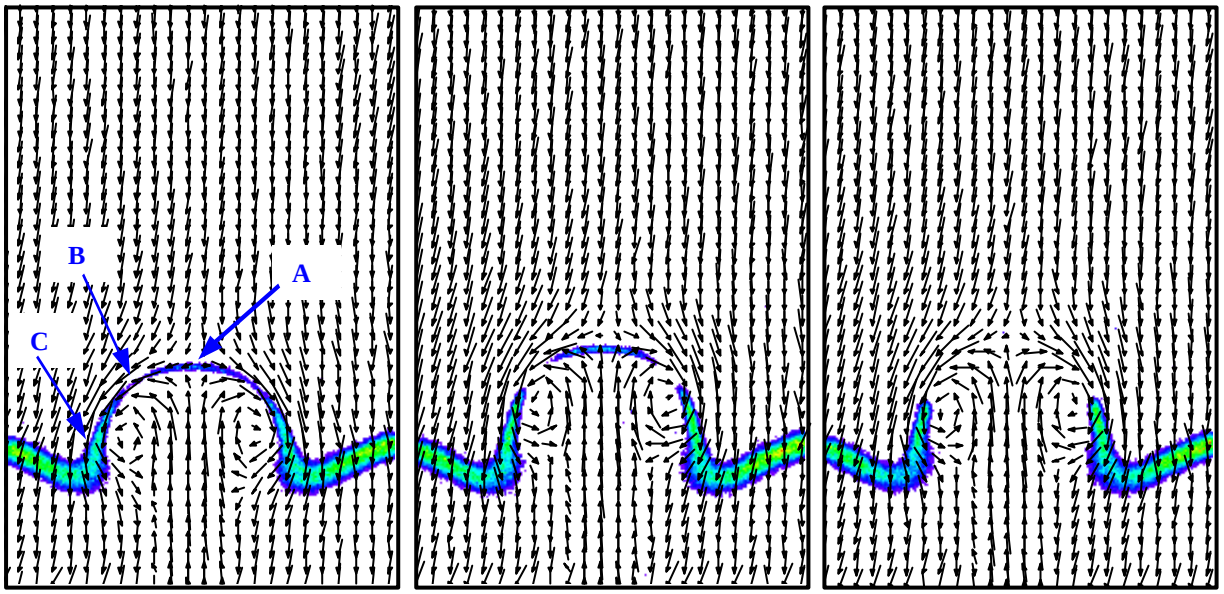

Fig. 5 Simultaneous OH-PLIF and velocity distribution showing the time resolution required to capture the flame extinction. Images progress in time from left to right and are spaced 0.3 ms apart.

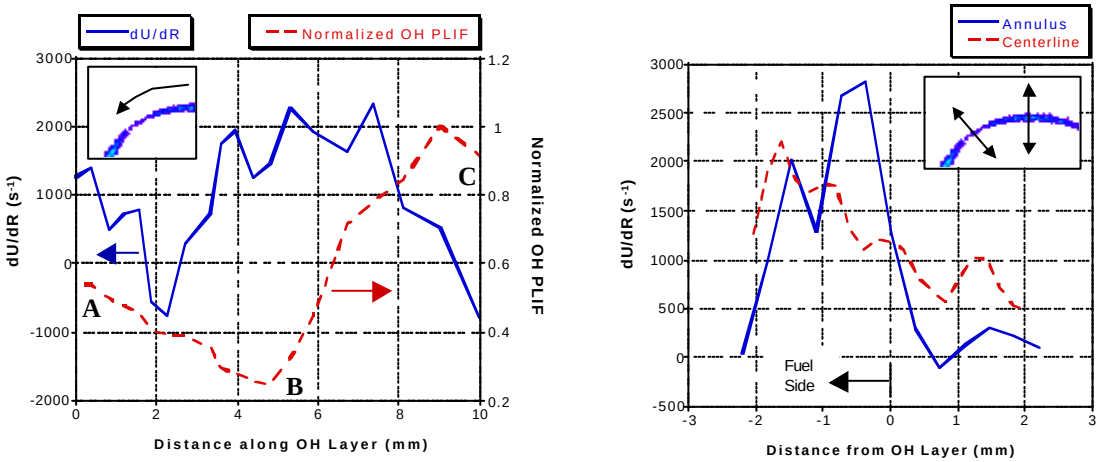

(a) (b)

Fig. 6 (a) Velocity gradient normal to the flame surface (dU/dR) and normalized OH PLIF *along* the flame from Point A to Point C from the leftmost image of Fig. 5; (b) Velocity gradient normal to the flame surface measured *across* Points A (centerline) and B (extinction region) from the leftmost image of Fig. 5.